Chinese Chemical Letters 34 (2023) 108262

Contents lists available at ScienceDirect

Chinese Chemical Letters

journal homepage: www.elsevier.com/locate/cclet

# Real-time monitoring flexible hydrogels based on dual physically cross-linked network for promoting wound healing

Le Hu[a,1], Yuxin Wang[a,1], Qing Liu[a], Man Liu[a], Faming Yang[a], Chunxiao Wang[a], Panpan Pan[a,*], Lin Wang[a], Li Chen[c], Jingdi Chen[a,b,*]

[a] Marine College, Shandong University, Weihai 264209, China
[b] Shandong Laboratory of Advanced Materials and Green Manufacturing, Yantai 265599, China
[c] College of Biological Science and Technology, Fuzhou University, Fuzhou 350108, China

ARTICLE INFO

*Article history:*
Received 19 November 2022
Revised 16 February 2023
Accepted 22 February 2023
Available online 2 March 2023

*Keywords:*
Conductive hydrogel
Dual cross-linked network
Antimicrobial activity
Real-time monitorin
Wound healing

ABSTRACT

To achieve smart and personalized medicine, the development of hydrogel dressings with sensing properties and biotherapeutic properties that can act as a sensor to monitor of human health in real-time while speeding up wound healing face great challenge. In the present study, a biocompatible dual-network composite hydrogel (DNCGel) sensor was obtained *via* a simple process. The dual network hydrogel is constructed by the interpenetration of a flexible network formed of poly(vinyl alcohol) (PVA) physical cross-linked by repeated freeze-thawing and a rigid network of iron-chelated xanthan gum (XG) impregnated with $Fe^{3+}$ interpenetration. The pure PVA/XG hydrogels were chelated with ferric ions by immersion to improve the gel strength (compressive modulus and tensile modulus can reach up to 0.62 MPa and 0.079 MPa, respectively), conductivity (conductivity values ranging from $9 \times 10^{-4}$ S/cm to $1 \times 10^{-3}$ S/cm) and bacterial inhibition properties (up to 98.56%). Subsequently, the effects of the ratio of PVA and XG and the immersion time of $Fe^{3+}$ on the hydrogels were investigated, and DNGel3 was given the most priority on a comprehensive consideration. It was demonstrated that the DNCGel exhibit good biocompatibility *in vitro*, effectively facilitate wound healing *in vivo* (up to 97.8% healing rate) under electrical stimulation, and monitors human movement in real time. This work provides a novel avenue to explore multifunctional intelligent hydrogels that hold great promise in biomedical fields such as smart wound dressings and flexible wearable sensors.



Flexible electronic equipment with excellent electromechanical and biological therapeutic characteristics is needed to monitor human physiological activities and promote wound healing. At present, hydrogel, as a multifunctional wet material, shows great potential in health monitoring and wound treatment. Zhang *et al.* mention 3D printing hydrogels in some applications, such as assistive technologies for rehabilitation, training and regenerative biomedicines [1]. Hydrogels are composed of a three-dimensional polymer network with high water content and are moist, soft, and ion-rich [2–4]. The mechanical properties are similar to those of biological tissues and are biocompatible [5–7]. Despite the high potential of hydrogels as multifunctional materials, the low mechanical strength of hydrogels is a drawback for practical applications. To improve the mechanical strength of hydrogels, researchers have enhanced the mechanical strength of hydrogels by designing double-network hydrogels. Dual-network hydrogels can integrate and optimize the advantages of each network to obtain better properties than the corresponding single networks [8,9]. Two contrasting networks, crosslinked by covalent or non-covalent bonds, respectively, synergize with each other to enhance the toughness and intensity of hydrogels [10,11]. Chen *et al.* prepare hydrogels with favorable mechanical strength which the unique cross-linked network formed through hydrogen-bonding, metal-ligand coordination and ionic interaction [12]. As a new type of conductive material, conductive hydrogel not only has conductivity but also has many characteristics of hydrogel, such as flexibility and biocompatibility. These characteristics are conducive to its application in the fields of skin dressing, drug release, biosensors, and flexible wearable electronic devices. Conductive hydrogels are generally divided into polyelectrolyte-doped type, inorganic conductive components (metal nanoparticles, carbon-based nanoparticles) added type, conductive polymer composite type, and so on.

* Corresponding authors.
*E-mail addresses:* pppan@sdu.edu.cn (P. Pan), jdchen@sdu.edu.cn (J. Chen).
[1] These authors contributed equally to this work.

https://doi.org/10.1016/j.cclet.2023.108262
1001-8417/

Due to its excellent biocompatibility, hydrophilicity, and biodegradability, poly(vinyl alcohol) (PVA) hydrogel has been extensively researched and used in the field of wound dressings [13]. But the majority of PVA hydrogels created by either physical entanglement or chemical cross-linking are weak, lack tensile strength, have low elastic modulus, and lose a lot of water [14,15]. To expand the application of PVA hydrogels, the above problems should be solved. 3D chitosan/PVA/gelatin hydrogels containing honey prepared by the freeze-thaw method have appropriate mechanical properties and antimicrobial activity and biocompatibility [16]. However, their tissue adhesion is weak and their mechanical properties are less than ideal. Gong *et al.* prepare a double network hydrogel consisting of PVA and poly(acrylamide-*co*-acrylic acid) (PAM-*co*-PAA) with ultra-high tensile strength (~1230 kPa) and large elongation (>5-fold) [17]. However, it is still challenging to develop a new hydrogel with good mechanical toughness and tensile capacity as well as some additional features such as electrical conductivity, pH sensing and self-healing.

Xanthan gum (XG) is biocompatible, biodegradable, bioadhesive and non-toxic, and is used for environmental sensing, water purification and antimicrobial activity [18,19]. XG can not only produce coordination effect with biological macromolecules to form higher viscosity or gel, but also form physical crosslinked hydrogels by complexing with transition metal ions with empty orbits. It is shown that the cross-linking of XG molecular chains with $Fe^{3+}$ can be a simple and effective method to make XG hydrogels [20]. More interestingly, the hydrogels can exhibit sol-gel conversion under UV irradiation after the addition of sodium lactate to the XG system [21]. However, the mechanical properties of pure XG are poor and unstable. Rong *et al.* designed a dual physically cross-linked polyacrylamide/xanthan gum (PAM/XG) DN hydrogel with divalent cation ($Ca^{2+}$) cross-linked XG as the first network and surfactant (SDS)-containing PAM as the second network. The DN hydrogel appeared high strength and toughness, self-healing properties [22]. Nevertheless, the antibacterial property of double-network hydrogel needs to be further explored.

In addition, when ionic gel sensors are applied to the human body, human sweat or moist environments tend to harbor harmful bacteria that pose a potential threat to human health, so it is desired to introduce antibacterial functions to ionic gel sensors [23,24]. Iron has a number of clinical uses, including ferrous sulfate vitamin complex for chronic bleeding disorders and ferrous fumarate for iron deficiency anemia. It was found that both Gram-negative and Gram-positive bacteria can adsorb $Fe^{3+}$ and rapidly reduce $Fe^{3+}$ to $Fe^{2+}$ under aerobic conditions. The generated $Fe^{2+}$participates in the Fenton reaction and generates hydroxyl radicals, which cause cell membrane lipid peroxidation, protein damage and DNA damage, among which DNA damage is the most serious [25]. Excess $Fe^{2+}$ can also catalyze the generation of reactive oxygen species (ROS) in large quantities through the Haber-Weiss reaction, which can have a certain inhibitory effect on bacterial growth [26].

Here, the hydrogel is fabricated by physical cross-linking in two steps (Scheme 1). XG and PVA are physically cross-linked internally by freeze-thawing using hydrogen bonds and crystalline regions to form the first flexible network. The XG is then physically cross-linked by soaking in a solution containing iron ions to form a ligand bond with iron ions to form a second rigid network. The dual-network DNCGel hydrogel was prepared by adjusting their ratio to obtain the optimal material. The dual-network structure not only can establish a stable network to enhance the mechanical properties (compressive modulus and tensile modulus can reach up to 0.62 MPa and 0.079 MPa, respectively) but also can improve the sensitivity of the hydrogel through the interaction of amphoteric ionic functional groups with metal ions. The hydrogel's exceptional conductivity gives the wound dressing a sensing capability that is

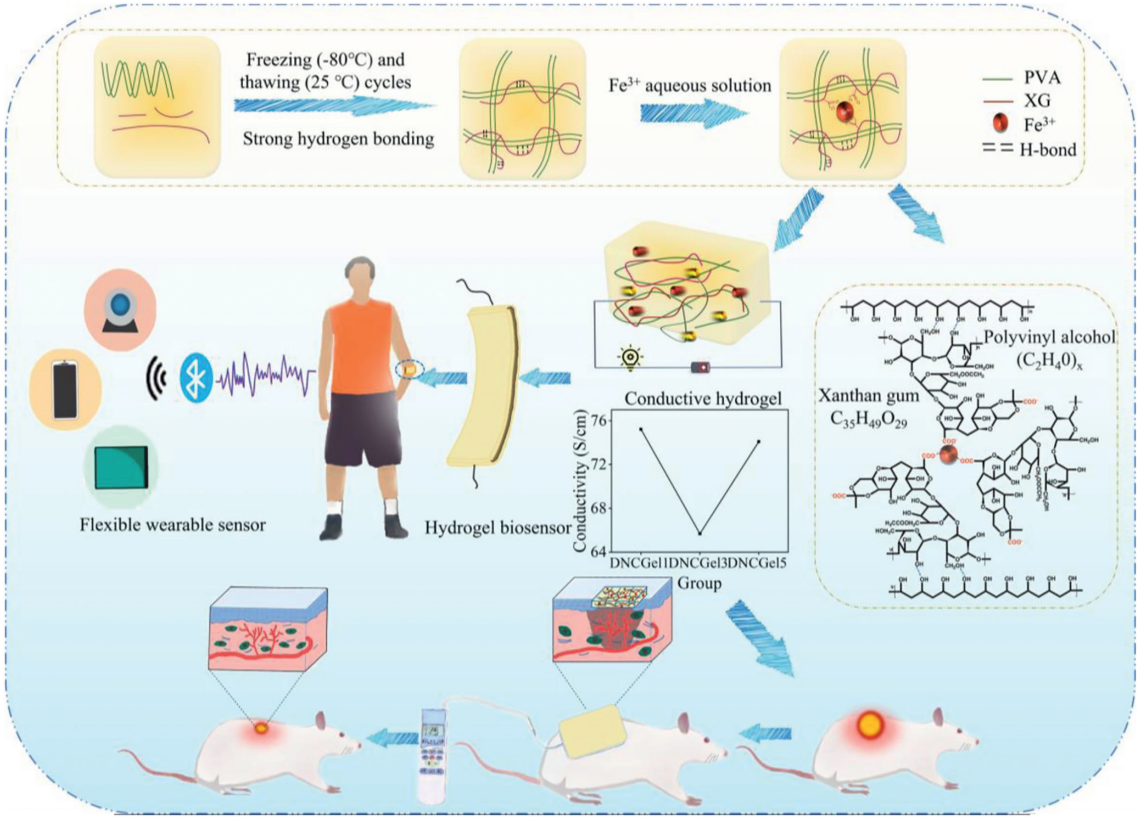


**Scheme 1.** The formation mechanism of dual network conductive hydrogels and their potential applications such as flexible wearable sensors, smart wound dressings.

helpful for accurate and real-time monitoring of wound conditions. At the same time, the sensor based on ionic gel has obvious antibacterial ability and acceptable cell compatibility, which ensures the biosafety of the material in wound recovery. Full-thickness skin wound model experiment *in vivo* proves that DNCGel hydrogel under electrical stimulation can promote wound healing. Therefore, this hydrogel has a high potential for health detection and wound healing.

In this paper, PBS buffer was selected to simulate the solution in a human physiological environment and the swelling rate was characterized by the 84 h weight change of the double network hydrogels. All gels have reached the swelling equilibrium within 84 h (Fig. 1A). XG content is a key factor affecting the swelling rate of the material. The higher the XG content, the longer it takes for the material to reach swelling equilibrium and the lower the swelling rate. This is because the XG concentration increases; it has more hydrogen bond formation with PVA, and the degree of hydrogel cross-linking increases. In addition, the time of immersion in $Fe^{3+}$ also affects the swelling rate, and the shorter the time of immersion in $Fe^{3+}$ for hydrogels with high XG content, the higher the swelling rate. This may be due to the chelation reaction between $Fe^{3+}$ and XG, resulting in smaller pores of the hydrogel, which makes it difficult to absorb water. The degradation rate of the hydrogel gradually increased over time (Fig. 1B). The mass loss rate of hydrogel degradation significantly decreased when XG content was increased, indicating that the hydrogen bond between XG and PVA in hydrogel could significantly reduce the degree of gel degradation. In addition, the degradation rate of the hydrogel decreased with the soaking time of $Fe^{3+}$, because as the soaking duration of the $Fe^{3+}$ rose, the density of crosslinking sites created by the coordination of XG and $Fe^{3+}$ increased, thus enhancing the structural stability.

The higher the XG content, the higher the compressive modulus and tensile modulus, which can reach up to 0.62 MPa and 0.079 MPa, respectively (Figs. 1C and D). PVA/XG hydrogel's hydroxyl group's stretching vibration peak shifts to a high wave number, and the intensity of the hydroxyl group peak increases obviously, about 3450 $cm^{-1}$. This is caused by the vibration absorption of intermolecular or intramolecular hydrogen bonds of hydroxyl groups in molecular chains. It shows that the freezing-thawing cycle can make the molecular chains of gel produce hydrogen bonds to form physical cross-linking, which can improve the mechanical properties of the hydrogel. The vibrational peak of the ether bond is at 1110 $cm^{-1}$, and this peak tends to broaden after cross-linking, indicating that new ether bonds may be formed. 1626 $cm^{-1}$ is the peak of the associated carbonyl group, which is stronger than XG's peak. It may be due to the reduction of intermolecular distance after cross-linking, which strengthens the conjoining effect. The characteristic absorption peak of -C=O in pyruvate in PVA/XG@$Fe^{3+}$ hydrogels shift to lower wave numbers with a sharp peak at 1606 $cm^{-1}$. The absorption peak near 1730 $cm^{-1}$ is shifted to 1725 $cm^{-1}$. It is speculated that this is caused by the decrease of electron cloud density on -C=O due to the coordination of $Fe^{3+}$ with -COO-. It is possible that the high concentration of XG caused the concentration of PVA to decrease, which in turn caused the intensity of the hydroxyl peak of the PVA/XG7@$Fe^{3+}$ hydrogel to diminish. This eventually leads to a decrease in H bonding as shown in Fig. S3B (Supporting information). This indicates that the hydrogel has good hardness, tensile strength and elasticity. The results reflect the tensile properties of the flexible network of the first physical cross-linking of the hydrogel, which can effectively realize the energy dissipation of the hydrogel during the tensile process through reversible hydrogen bonding, thus enhancing its tensile properties (Fig. 1E). The network of XG is rigid, the higher the network cross-linking, the greater the stiffness of the hydrogel. On the other hand, it shows that the second rigid network can improve the tensile breaking strength of hydrogel and endow hydrogel with excellent mechanical properties (Fig. 1F). While the physically cross-linked network of PVA is elastic, the hydrogel becomes more elastic as concentration increases. Then the ratio of PVA and XG can be adjusted to synthesize the hydrogel with the desired hardness, and for this purpose, the dual network hydrogel also adds more potential for application [27,28]. As the soaking time of $Fe^{3+}$ increases, the elastic modulus and compressive modulus of hydrogels show a trend of increasing and then decreasing. The amount of $Fe^{3+}$ as a cross-linking agent affects the degree of cross-linking of the gel. As the cross-linking agent concentration rises, the degree of chemical cross-linking of the gel becomes larger, the internal structure is tighter, the pores are uniformly present, and thus the mechanical strength increases while at higher crosslinking densities, the movement of PVA and XG chains is restricted affecting the mechanical properties.

The primary consequence of skin conditions like burns and scalds is bacterial infection [29,30]. Bacteria continue to infect wounds and subcutaneous tissues during the healing process by proliferating and releasing toxins [31]. The bacterial surface is negatively charged due to polysaccharide excess amides (related positively charged substances). The positively charged hydrogel will capture negatively charged bacteria (electrostatic adsorption). It is reported that $Fe^{3+}$ can be absorbed by gram-positive bacteria and gram-negative bacteria and rapidly reduced to $Fe^{2+}$. The resulting $Fe^{2+}$ can produce rich hydroxyl radical (OH), which can cause lipid peroxidation of cell membrane, protein dysfunction and even cell death (Fig. 2A). The results showed that PVA/XG@$Fe^{3+}$ hydrogel had good antibacterial activity against *E. coli* and *S. aureus*. In the figure, the hydrogel is in contact with the inhibitory zone on the agar plate (Fig. 2B), and the results of viable bacteria count after co-culture with the hydrogel-containing bacterial solution (Fig. 2C). The existence of $Fe^{3+}$ makes PVA/XG@$Fe^{3+}$ hydrogel have better antibacterial activity. In the bacteriostatic circle experiment, all three hydrogels can produce an obvious bacteriostatic circle. However, after co-culture with DNCGel3 and DNCGel5, almost no bacterial colonies were observed (Fig. 2D). Therefore, PVA/XG@$Fe^{3+}$ hydrogel can potentially be used as a sensor with antibacterial properties, which can inhibit bacteria and prevent tissue infection without antibiotics.

The flame absorption method was used to analyze the release of ions into the solution during the soaking process of hydrogel (Fig. 3A). The concentration of $Fe^{3+}$ increased rapidly at the beginning, and then gradually increased slowly. The final $Fe^{3+}$ concentration is 1.86–21.03 mg/L. The release content of iron ions is also higher than the concentration of ions which can promote endothelial cell proliferation (1.59–12.7 μg/L), which indicates that bioactive hydrogel materials can be obtained by doping iron ions. The hydrogel can promote the proliferation of endothelial cells by releasing active ions, which also provides the possibility for the subsequent use of polymer composite.

Skin is a tissue sensitive to electrical signals, with conductivity values ranging from $1 \times 10^{-7}$ S/cm to $2.6 \times 10^{-3}$ S/cm [32]. PVA/XG@$Fe^{3+}$ hydrogels have great electrical conductivity due to the migration of anions and cations inside the hydrogel network, which is similar to that of skin. Therefore, PVA/XG@Fe can be applied to human skin as a conductive dressing [32]. With the increase of $Fe^{3+}$ immersion time, the iron salt content in the hydrogel increased, which helped the iron ions in the polymer matrix migrate. Therefore, the conductivity of DNCGel3 hydrogel is higher than that of DNCGel1 hydrogel (Fig. 3B). In addition, the content of the aqueous solution as an important migration medium for conductive particles is also critical to the conductivity of the material. The lower conductivity of DNCGel5 hydrogels than DNCGel3 hydrogels indicates that the low water content of the system directly affects the internal ion migration, which in turn causes an

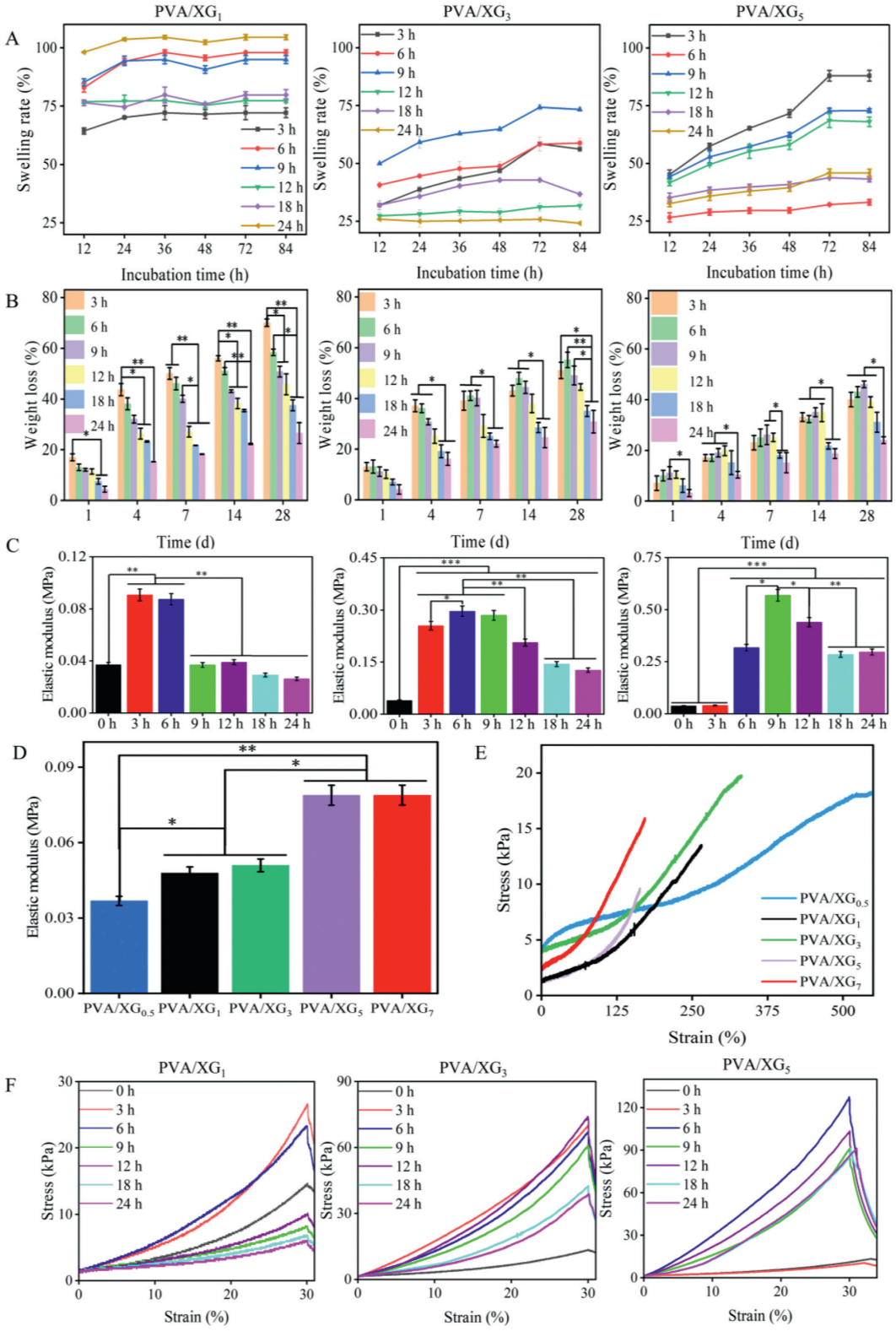


**Fig. 1.** The compression experiments (A), modulus of compressibility (B), tensile curve of tensile (C), and tensile modulus (D), the swelling rate (E) and the weight loss (F) of hydrogels ($n = 5$, $^{*}P < 0.05$, $^{**}P < 0.01$, $^{***}P < 0.001$).

increase in system resistance and a reduction in electrical conductivity. Because DNCGel3 has the best conductivity and is similar to skin conductivity, DNCGel3 is finally selected for strain sensitivity test and human motion monitoring.

The cyclic Load-unload mechanical tests revealed efficient recovery of the conductive hydrogels after ten consecutive cyclic tensile tests at 100% strain. The iron chelating network, the first of a double network structure, is relatively rigid, brittle and tightly cross-linked in terms of the second network, dissipating a large amount of energy during deformation. The PVA network is extensible and loosely cross-linked, protecting the integrity of the hydrogel after the first network was broken. The results showed (Fig. 3C)

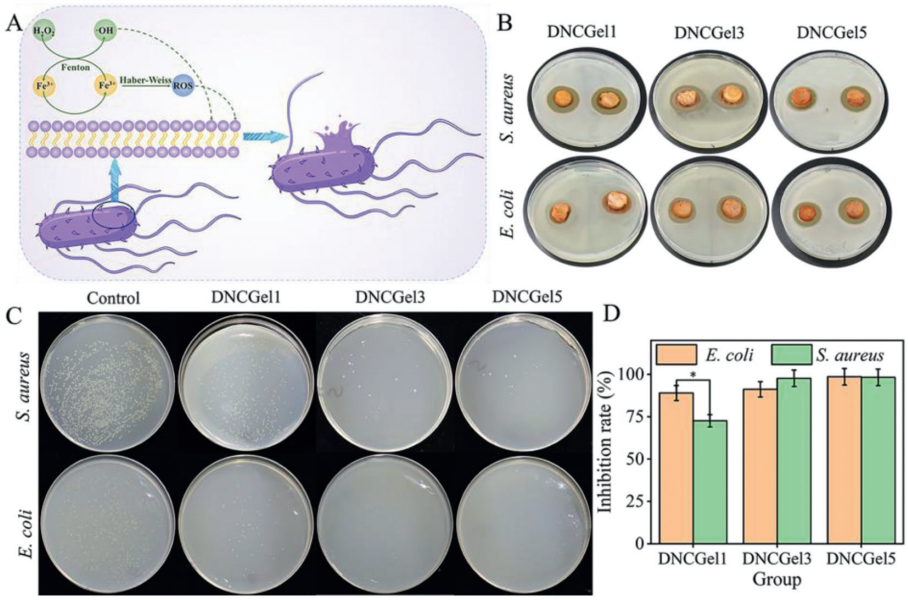


**Fig. 2.** (A) Antibacterial mechanism of hydrogel. (B) The antibacterial performance of DNCGel1, DNCGel3 and DNCGel5 hydrogel against *E. coli* and *S. aureus*. (C) Count of viable bacteria after co-culture. (D) Photographs showing the bacterial culture plates of *S. aureus* and *E. coli* upon 12 h of exposure to the control and various hydrogels ($n = 5$, $^{*}P < 0.05$).

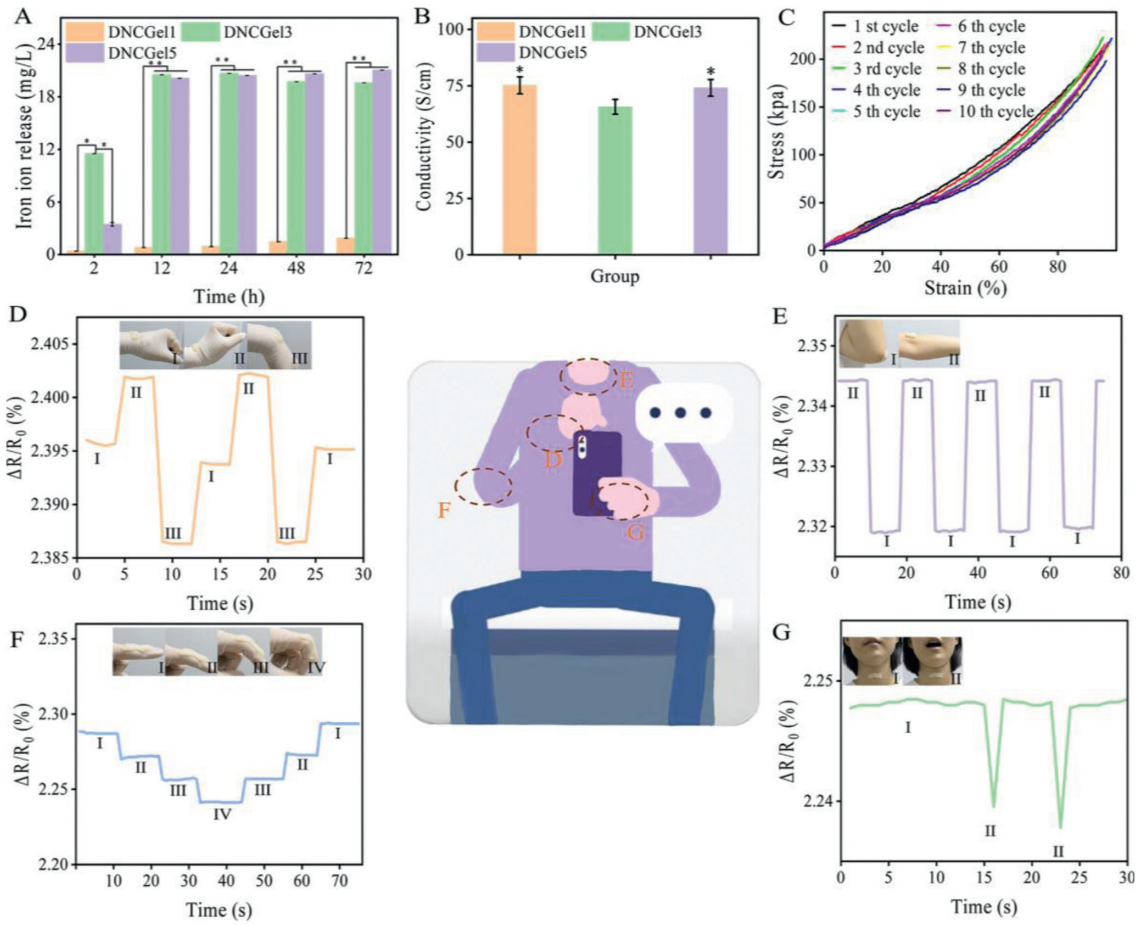


**Fig. 3.** Iron ion release (A) and conductivity (B) of the DNCGel1, DNCGel3 and DNCGel5 hydrogel. (C) Ten cycles of stretching at 100% strain. Monitoring of joint movement and electrochemical properties of the DNCGel3 hydrogel: Wrists bending (D), pronouncing "Ah" (E), elbows bending (F) and fingers bending (G) ($n = 5$, $^{*}P < 0.05$, $^{**}P < 0.01$).

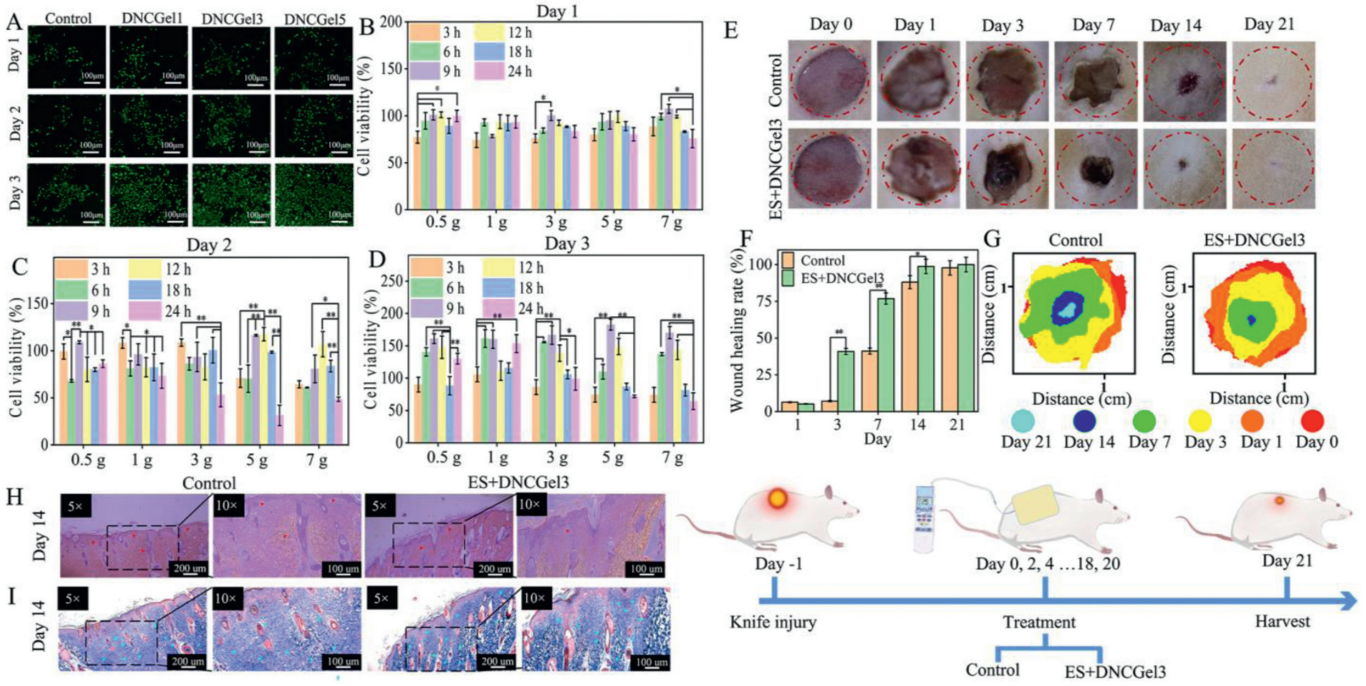


**Fig. 4.** (A–C) Cell proliferation on the hydrogel for 3 days culture in the leaching solution using the CCK-8 assay. (D) AO/EB fluorescence staining images of cells after 3 days of culture in the leaching solution. (E) Electrostimulation of rats with full-thickness skin loss wounds, and photographs of the differently-treated wounds on days 0, 1, 3, 7, 14 and 21. (F) The wound area (%) decreased within 21 days under the two treatments. (G) Wound area changes under the two treatments. (H) H&E staining and (I) Masson staining in the wound area on day 14. The rectangular area in the tricolor dyed images of H&E and Masson is enlarged on its right side. The red triangle in H&E indicates inflammatory factors; The cyan triangle in Masson's tricolor stained image represents the newborn collagen ($n = 5$, $^{*}P < 0.05$, $^{**}P < 0.01$).

that the double network structure inside the conductive hydrogel formed an effective energy dissipation mechanism and exhibited fatigue resistance. The hydrogel sensor can quickly and accurately respond to limb movements such as fingers (Fig. 3D), bending elbows (Fig. 3E) and wrists (Fig. 3F). For periodic limb movements, the hydrogel sensor can generate corresponding periodic electrical signals. When the hydrogel is attached to the finger, the bending angle of the finger changes from 0 to 90, and each angle stays for a few seconds. Different angles correspond to different relative resistance changes, and the relative resistance can remain stable during the stay, which is mainly due to the dynamic physical action inside the hydrogel and its stable ion mobility. In addition, a hydrogel can also respond well to different speech states (Fig. 3G). Sticking the hydrogel on the throat can distinguish the different states of vocalization from unvoiced. The outcomes of the experiment demonstrate that hydrogel is highly sensitive to human movements, and it is an ideal candidate material for the next generation of flexible electronics devices.

Conducive hydrogels with great biocompatibility are essential for achieving practical applications because sensors used to detect human activity are frequently in contact with the human body [33]. The cytotoxicity of the hydrogel was examined using the CCK-8 assay and AO/EB staining to assess hydrogels' biocompatibility and to analyze the interaction between cells and their environment. All hydrogels sustained cell survival and were able to preserve cell morphology for 3 days, according to AO/EB staining plots (Fig. 4A). The findings of the CCK-8 assay (Figs. 4B–D) demonstrated that the relative cell growth on the same hydrogel rate (RGR) increased with increasing incubation time. After 3 days of incubation, the cell viability of hydrogels soaked with $Fe^{3+}$ for 3 h, 6 h and 12 h was significantly higher than the other groups, with RGR values higher than 100% and up to 182%, indicating very low cytotoxicity and good biocompatibility. The surface structure of the hydrogel is a key factor in cell attachment and subsequent proliferation [34]. In SEM observation studies, the microstructure of PVA/XG@$Fe^{3+}$ hydrogel was a homogeneous three-dimensional network structure, which provided a good environment for cell attachment. The increase in cell proliferation may originate from the good cell attachment rate. Therefore, a certain concentration of $Fe^{3+}$ could improve the biocompatibility of the hydrogel by enhancing the hydrogel's structure.

The therapeutic effect of hydrogel on rat wounds was evaluated. It was reported that electrical stimulation can accelerate wound healing through promoting the migration, proliferation of epithelial and secretion of collagen and increasing fibroblast ingrowth and collagen fiber arrangement. The wounds of rats in each group gradually healed during the observation period, and the wound healing process showed that DNCGel3 hydrogel electrostimulation therapy recovered fastest from wound infection (The healing rate is as high as 97.8%.) (Figs. 4E–G). In addition, H&E staining and Masson staining of rat skin wound tissues at different times showed the effect of the hydrogel at each major healing stage (Figs. 4H and I). On day 3, compared to the negative control group, the wound inflammatory cells were sparse in all groups, effectively suppressing the inflammatory response. Granulation tissue was thicker. On day 7, wounds in all groups were closed with a large amount of connective tissue compared to the negative control group as shown in Fig. S5 (Supporting information). On day 14, wounds in the DNCGel3 hydrogel group under electrical stimulation could all form regular epithelial cells and fibroblasts with more regular blood arteries, hair follicles, and connective tissue, similar to normal skin tissue, compared with other groups. To some extent, the size and density of collagen fibers can indicate how well new tissues are forming and mending. The development of collagen fibers and fibroblasts is directly tied to the wound healing process. After 21 days, collagen deposition (blue staining area) occurred in both groups as shown in Fig. S5. It is worth noting that DNCGel3 under electrostimulation therapy has the greatest collagen content and best fiber organization, especially on the seventh day, it can be observed that the collagen fibers from the wound are arranged

regularly and orderly, which further proves its powerful wound-healing effect.

In this study, we prepared a DNCGel bio-dressing with sensing function through a simple process. This unique dual network structure is composed of a physically cross-linked flexible network formed by repeated freeze-thawing of PVA and a rigid network created by $Fe^{3+}$-chelated XG that penetrates each other. The hydrogel possesses desirable mechanical properties (The compressive modulus and tensile modulus can reach up to 0.62 MPa and 0.079 MPa, respectively.), fatigue resistance, and swelling properties (24.14%−104.56%), which promote the preservation of stable structure and material function during healing of wounds. The antimicrobial activity of the hydrogel can effectively reduce inflammation and avoid pollution of environment caused by the use of antibiotics. The effective proliferation of HUVECs cells confirmed the good biocompatibility of the material and ensured the biosafety of the material in healing of wound. *In vivo* whole skin wound model results showed that DNCGel3 hydrogel has a positive effect on healing of wound (the healing rate is as high as 97.8%). Its excellent electrical conductivity (conductivity values ranging from $9 \times 10^{-4}$ S/cm to $1 \times 10^{-3}$ S/cm) conferred sensory properties to the hydrogel and successfully monitored multiple human activities. All of these findings imply that DNCGel3 hydrogel can be successfully employed as a sensory biological dressing to track different human activities while accelerating wound healing.

## Declaration of competing interest

The authors declare that they have no known competing financial interests or personal relationships that could have appeared to influence the work reported in this paper.

## Acknowledgments

This work was supported by Physical Chemical Materials Analytical & Testing Center of Shandong University at Weihai, Natural Science Foundation of Shandong Province (No. ZR2022QD057), Open Project Fund for Hubei Key Laboratory of Oral and Maxillofacial Development and Regeneration (No. 2021kqhm003), State Key Laboratory of Advanced Technology for Materials Synthesis and Processing (Wuhan University of Technology), and the Science Fund of Shandong Laboratory of Advanced Materials and Green Manufacturing (Yantai, No. AMGM2021F02).

## Supplementary materials

Supplementary material associated with this article can be found, in the online version, at doi:10.1016/j.cclet.2023.108262.

## References

[1] A. Zhang, F. Wang, L. Chen, et al., Chin. Chem. Lett. 32 (2021) 2923–2932.
[2] D. Gan, T. Xu, W. Xing, et al., Adv. Funct. Mater. 29 (2019) 1805964.
[3] P. Pan, T. Zhang, Q. Yue, et al., Adv. Sci. 7 (2020) 2000443.
[4] K. Huang, Q. Ou, Y. Xie, et al., ACS Biomater. Sci. Eng. 5 (2019) 4037–4047.
[5] Y. Wang, F. Chen, Z. Liu, et al., Angew. Chem. Int. Ed. 58 (2019) 15707–15711.
[6] D. Seliktar, Science 336 (2012) 1124–1128.
[7] P. Pan, X. Chen, H. Xing, et al., Chin. Chem. Lett. 32 (2021) 2159–2163.
[8] L. Hu, L. Zou, Q. Liu, et al., Int. J. Biol. Macromol. 215 (2022) 377–386.
[9] Y. Liu, M. Zhu, M. Meng, et al., Chin. Chem. Lett. 34 (2023) 107583.
[10] C. Zhang, B. Wu, Y. Zhou, et al., Chem. Soc. Rev. 49 (2020) 3605–3637.
[11] Z. Jiang, Y. Wang, G. Xu, et al., Chin. Chem. Lett. 33 (2022) 1011–1016.
[12] S. Chen, L. Yin, L. Liu, N. Zhang, D. Dong, Chin. Chem. Lett. 32 (2021) 3133–3136.
[13] Y. Li, H. Zheng, Y. Liang, et al., Chin. Chem. Lett. 33 (2022) 5030–5034.
[14] E.A. Kamoun, E.S. Kenawy, X. Chen, J. Adv. Res. 8 (2017) 217–233.
[15] Y. Mao, Z. Xu, Z. He, J. Wang, Z. Zhu, Chin. Chem. Lett. 34 (2023) 107461.
[16] A. Shamloo, Z. Aghababaie, H. Afjoul, et al., Int. J. Pharm. 592 (2021) 120068.
[17] Z. Gong, G. Zhang, X. Zeng, et al., ACS Appl. Mater. Interfaces 8 (2016) 24030–24037.
[18] C. Alvarez Lorenzo, B. Blanco Fernandez, A.M. Puga, A. Concheiro, Adv. Drug Delivery Rev. 65 (2013) 1148–1171.
[19] Q. Zhang, X.M. Hu, M.Y. Wu, et al., React. Funct. Polym. 136 (2019) 34–43.
[20] V.E.S.F Garcıá Ochoa, J.A. Casas, E. Gómez, Biotechnol. Adv. 18 (2000) 549–579.
[21] M. Kang, O. Oderinde, S. Liu, et al., Carbohydr. Polym. 203 (2019) 139–147.
[22] N. Yuan, L. Xu, H. Wang, et al., ACS Appl. Mater. Interfaces 8 (2016) 34034–34044.
[23] N. Jiang, X. Chang, D. Hu, et al., Chem. Eng. J. 424 (2021) 130418.
[24] B. Zhang, Y. Guo, J. Huo, et al., Chem. Eng. J. 382 (2020) 123055.
[25] J.A. Imlay, Nat. Rev. Microbiol. 11 (2013) 443–454.
[26] R.Y. Pelgrift, A.J. Friedman, Adv. Drug Delivery Rev. 65 (2013) 1803–1815.
[27] C.E. Brunchi, M. Bercea, S. Morariu, M. Avadanei, Eur. Polym. J. 84 (2016) 161–172.
[28] J. Zhou, F. Zhuo, X. Long, et al., Chem. Eng. J. 447 (2022) 137259.
[29] L. Wang, Y. Li, L. Lin, R. Mu, J. Pang, Carbohydr. Polym. 236 (2020) 116045.
[30] G.G. Mohamed, A.A. El Sherif, M.A. Saad, S.E.A. El Sawy, S.M. Morgan, J. Mol. Liq. 223 (2016) 1311–1332.
[31] R. Ricciardi, F. Auriemma, C. De Rosa, F. Lauprêtre, Macromolecules 37 (2004) 1921–1927.
[32] S. Liu, F. Yao, M. Kang, et al., Mater. Des. 113 (2017) 232–239.
[33] T. Chen, Y. Chen, H.U. Rehman, et al., ACS Appl. Mater. Interfaces 10 (2018) 33523–33531.
[34] J. Huang, J. Ren, G. Chen, et al., J. Nanomater. 2017 (2017) 1–10.